Biophysical Chemistry 16 (1982) 307–316
Elsevier Biomedical Press



# SOLUTION SCATTERING STUDIES OF DIMERIC AND TETRAMERIC SPECTRIN

M.H. REICH [a], Z. KAM [a], H. EISENBERG [a], D. WORCESTER [b], E. UNGEWICKELL [c] and W.B. GRATZER [c]

[a] *Polymer Research Department, Weizmann Institute of Science, Rehovot, Israel,* [b] *Institut Laue Langevin, Grenoble, France, and* [c] *Medical Research Council, Cell Biophysics Unit, King's College, Drury Lane, London WC2B 5RL, U.K.*

Received 22nd April 1982
Revised manuscript received 30th July 1982
Accepted 3rd August 1982

*Key words: Light scattering; X-ray scattering; Neutron scattering; Spectrin conformation*

The structure of spectrin dimers and tetramers in solution has been examined by light, low-angle X-ray and neutron scattering. The results show a good correspondence between the solution dimensions of these molecules and their appearance in the electron microscope after shadowing. The scattering profiles are not compatible with an extended rod-like character, but reflect the presence of a considerable degree of bending. The radii of gyration of the dimer and tetramer were determined to be 170 and 375 Å and the cross-section radii of gyration 14 and 12.3 Å, respectively. Both are thus long, thin, rather bent molecules, and the tetramer is twice the length of the dimer.

## 1. Introduction

Spectrin is the major protein of the membrane-associated cytoskeleton of the mammalian red cell. It contains two subunits, with molecular weights of about 250 000 and 230 000, associated as heterodimers. In the cell it is present almost entirely in the form of a tetramer, containing two such heterodimers, associated head-to-head. In the electron microscope the heterodimer presents the appearance of an elongated molecule, in which two strands appear to be in contact at their ends and loosely coiled about one another [1,2]. The contour length in the electron microscope is about 950 Å. The tetramer is also extended, and about twice the length of the dimer. Other cytoskeletal proteins of similar molecular weight to that of the spectrin dimer are filamin and macrophage actin-binding protein, and these resemble spectrin in their gross features in the electron microscope after shadowing [3]. It was accordingly suggested that spectrin might be representative of a class of cytoskeletal proteins with common structural characteristics. These characteristics are presumed to be linked to their function in the cell, which in the case of spectrin is evidently to confer on the membrane the mechanical properties that allow it to undergo gross and reversible deformations of shape, without damage. The conformation of these proteins is therefore of considerable interest. Findings from electron microscopy are under some circumstances subject to artefacts of preparation. This applies to our own earlier results in which uranyl acetate negative staining was used [4]. The results obtained by Shotton et al. [1] by shadowing can be regarded as definitive, however. Scattering studies are required to determine whether the state of the molecule in solution corresponds to that on the grid after drying and shadowing, and to obtain a quantitative expression of the flexibility inherent in the chain conformation.

In an earlier publication we reported light scattering and other data on spectrin dimers [4]. The radius of gyration $R_g$ obtained from the light scattering was incorrectly stated because of an arithmetical error. This made it appear that these

results were in conflict with a subsequent light scattering study by Elgsaeter [5]. No such disagreement in fact exists, as shown by the slope of angular dependence of scattered intensity in fig. 2 of our previous paper. We have now attempted to obtain conformational information about both the dimer and tetramer of spectrin at higher resolution by the use of low-angle X-ray and neutron scattering, in addition to performing further light scattering measurements. The results lead to a more exact description of the structural character of spectrin in solution at physiological ionic strength.

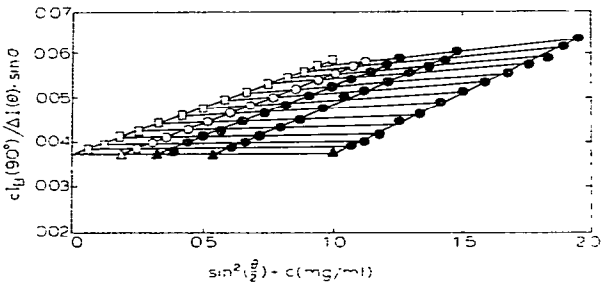


Fig. 1. Zimm plot of total light scattering intensity from spectrin tetramers. $I_B(90)$ is the scattering intensity at 90° from benzene. The lowest concentration (open circles) was a sample diluted from one used in the X-ray scattering measurements (see text). The zero angle and zero concentration extrapolations are denoted by triangles and squares, respectively.

## 2. Materials and methods

Spectrin was prepared from fresh human erythrocytes as described earlier [6] either by brief extraction at 37°C to give dimers or dialysis at 4°C for tetramers. After chromatography on Sepharose 4B the fractions containing pure dimer or tetramer were collected and concentrated by precipitating with ammonium sulphate and rapidly dissolving in the appropriate buffer in water or $^2H_2O$ [7]. Protein concentrations were determined spectrophotometrically, using a specific absorptivity ($E^{1\%}_{1\,cm}$ at 278 nm) of 10.7 [4]. Solutions were clarified by centrifugation at 80000 $g$ for 30 min. All measurements were done in 0.1 M NaCl, 0.05 M Tris, pH 7.8.

Total intensity light scattering and diffusion coefficient determinations were performed using a laser autocorrelation instrument (Malvern 4300, Precision Devices and Systems (U.K.) Ltd., Malvern), as previously described [8]. Measurements covered the angular range of scattering angles between 30 and 160°. (Scattering angles for light scattering are conventionally expressed in terms of $\theta$ and those for X-ray scattering of $2\theta$; we shall use $\theta$ throughout.) The temperature was maintained at 10–12°C. Under these conditions interconversion of dimer and tetramer is immeasurably slow [6]. A part of the solution used for X-ray scattering was diluted and used for the lowest concentration data on the light scattering Zimm plot (fig. 1).

The X-ray source was a Philips Cu X-ray tube with a fine line focus of 0.4 × 8 mm. As the system is oriented at an angle of 6° to the anode, the apparent focus seen by the detector was 0.04 × 8 mm. The X-ray beam was partially monochromatized by a nickel filter which reduced the intensity of $CuK_\beta$ and continuous background radiation. Beam collimation was provided by an uncoated quartz mirror focussing device [9], which monochromatized the beam further. A series of slits were used to reduce parasitic scattering. Beam height collimation was provided by two 4-mm high slits 32 cm apart, one just after the source and the other at the sample holder. The detector aperture height was also 4 mm. The measured half-width at the half-height of vertical divergence was about 14 mrad. Samples were contained in a 1 mm diameter quartz capillary in a thermostatically controlled holder. The temperature was maintained at 10–12°C. The scattered X-rays were detected with a 5 cm long Borkowski-Kopp position-sensitive detector, the position histogram being accumulated by a Varian minicomputer. The resolution of the detector was better than 0.3 mm. The distance between sample and detector was 78 cm for measurements on the dimer and 50 cm for the tetramer. The beam width at the detector was also about 0.3 mm, giving a resolution of about 0.5 mrad. The beam stop used allowed measurements to be collected in the angular range $\theta = 1.3$–32 mrad for the dimers, corresponding to Bragg spacings $d = \lambda/\theta$ of 1200–48 Å, and values of $q^2$ (with

the scattering vector $q = (4\pi n/\lambda)\sin(\theta/2)$, where $\lambda$ is the wavelength in vacuo, i.e., $\lambda = 1.54$ Å for $CuK_\alpha$, and $n$ is the refractive index of the medium which is close to unity for X-rays) of $2.8 \times 10^{-5}$ to $1.7 \times 10^{-2}$ Å$^{-2}$. Data were collected for the tetramers in the range $\theta = 1.4$–$50$ mrad. Data points below 2.1 mrad, just outside the beam stop, were not used in the analysis because of the presence of parasitic scattering in this region.

Neutron scattering measurements at the D11 instrument of the Institut Laue Langevin of spectrin dimers were performed at a wavelength of 7.97 Å and a sample-to-detector distance of 10.525 m. Data were collected in the range of $q^2$ between $4.6 \times 10^{-5}$ and $7.6 \times 10^{-4}$ Å$^{-2}$. Pinhole collimation was used and the data therefore did not require correction for convolution effects. Scattered neutrons were detected using an area detector. Two samples of concentration 4.2 and 1.6 mg/ml were measured in $^2H_2O$ buffers containing 0.1 M NaCl, 0.01 M phosphate, p$^2$H 7.5.

## 3. Results and data analysis

### 3.1. Light scattering

The angular dependence of the total light scattering intensity for the dimers has been previously reported [4]. As already remarked, the corresponding radius of gyration was incorrectly given. The reciprocal scattering intensity, normalized to zero scattering angle so that $I(0)/I(q) = P^{-1}(q)$ (fig. 2. of ref. 4), does not exceed 1.1; we may therefore calculate the radius of gyration, $R_g$, from the limiting Zimm slope, by way of the relation

$$P^{-1}(q) = 1 + q^2 R_g^2/3 \qquad (1)$$

applicable in this case (cf. fig. 6 of ref. 10).

We find $R_g = 170 \pm 30$ Å, which agrees with the value obtained by Elgsaeter [5].

The Zimm plot obtained for the tetramers is shown in fig. 1. From the double intercept at $c = 0$ and $\theta = 0$ we calculate (cf. ref. 4) a weight-average molar mass of $1.06 \times 10^6$, which is within experimental error twice that of the dimer, viz., $0.47 \times 10^6$ as previously reported by us on the basis of light scattering, and $0.54 \times 10^6$ from the Svedberg equation.

To calculate the radius of gyration of the tetramer we cannot use the limiting slope (eq. 1), since $P^{-1}(q)$ exceeds 1.1 and reaches 1.5 in the experimental range (fig. 1). For values of $P^{-1}(q) < 1.75$, however, the equation for the limiting models of long rods and Gaussian coils coincides (cf. fig. 6 of ref. 10). Following this procedure we calculate $R_g = 375 \pm 40$ Å for the tetramer, which is twice the value for the dimer, within error.

### 3.2. X-ray scattering

The dependence of the excess (over solvent) X-ray scattering from a solution of particles is given for sufficiently low angles by the equation of Guinier [11], viz.,

$$I(q) = I(0)e^{-q^2 R_g^2/3} \qquad (2)$$

We take $R_g$ to be the same for all three scattering techniques. $I(0)$ is given by,

$$I(0) = K I_o (\partial\rho_{el}/\partial c)_\mu^2 Mc \qquad (3)$$

where $c$ is the solute concentration (g/ml), $M$ the molar mass of a solute particle, $(\partial\rho_{el}/\partial c)_\mu$ the electron density increment [12], $I_o$ the intensity of the primary beam and $K$ depends on the geometry of the scattering system, i.e.,

$$K = i_t/a^2 N_A \, d F \qquad (4)$$

where $i_t$ is Thomson's constant [13] for the scattering of an electron, $a$ the sample-to-detector distance, $N_A$ Avogadro's number, $d$ the path length of the sample and $F$ the area corresponding to one channel of the data acquisition histogram. $F$ is the product of detector height (assuming uniform quantum efficiency along this axis) and the width in the detector plane of a counting channel. At low salt concentrations and neglecting preferential interactions $(\partial\rho_{el}/\partial c)_\mu$ can be written as $(l_2 - l_1\phi'\rho_o)$ where $l_1$ is the number of solvent electrons per g of solvent and $l_2$ the number of solute electrons per g of solute, $\phi'$ an apparent specific volume [12,14] and $\rho_o$ the solvent density. $\phi'$ in this case is close to the partial specific volume $\bar{v}$ of the scattering particle. These equations are strictly valid in the

limit of vanishing protein concentration. However, because the X-ray measurements were made in the outer regions of the scattering curves and the protein concentrations were relatively low (< 5 mg/ml), the concentration-dependent effects are expected to be small.

$K$ can be determined explicitly or from a calibration (for a given experimental configuration) in terms of secondary standards such as solutions of particles of known molecular weight, concentration and electron density increment.

For long rods, $I(q)$ can be approximated in the range of scattering vectors such that $1/R_g < q < 1/R_c$ as [15]:

$$I(q) = I(0)(\pi/qL)e^{-q^2R_c^2/2} \tag{5}$$

where $L$ is the length of the rod and $R_c$ the radius of gyration of its cross-section. $R_c$ can be determined from an appropriate plot of $\ln(qI(q))$ vs. $q^2$ (cross-section plot). When the data are plotted in this fashion they approach an asymptote, the slope of which is $R_c^2/2$. Absolute calibration of scattering intensities is not required in this case.

The mass per unit length ($M/L$) is related to the intercept of the asymptote at zero angle of $qI(q)$: from eq. 5

$$\{qI(q)\}_{q\to 0} = I(0)\pi/L \tag{6a}$$

$$= KI_o\pi(\partial\rho_{el}/\partial c)_\mu^2 c(M/L) \tag{6b}$$

This relation can be used to determine $KI_c$ for a given system from a cross-section plot of solutions of rod-like particles of known $M/L$.

Due to the instrumental collimation, the measured scattered intensities must be corrected for the effect of convolution [16]. The convolution corrections can be made by deconvoluting the experimental curves or by convoluting simulated model scattering curves with the instrumental parameters. For the latter case, convolutions of the scattering function of cylinders [17] were used. As shown in fig. 2, for sufficiently large angles, the slopes of the asymptotes are not affected by the convolution. The convolution in this region introduces an approximately constant multiplier, $C_R$, which can be used to obtain the corrected value of $K$ directly from the measured value, $\bar{K}I_o$, i.e., $KI_o = \bar{K}I_oC_R$.

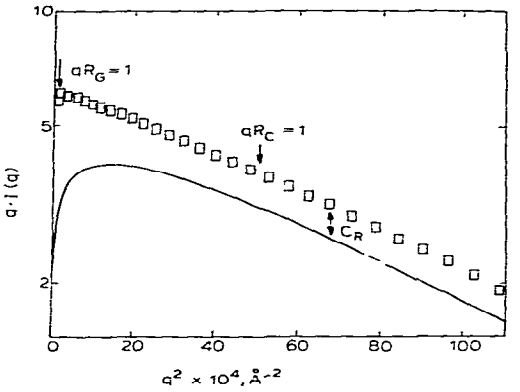


Fig. 2. The calculated low-angle X-ray scattering curve (squares) for a cylinder of radius of gyration 180 Å and cross-sectional radius of gyration 14 Å expressed as a cross-section plot. Also shown (continuous line) is the convolution of the calculated scattering curve with the slit geometry used. The ratio of the ordinates in the parallel region of the two curves ($qR_c > 1$) is denoted by $C_R$. The appropriate range for cross-section analysis lies between the arrows.

The value of $KI_o$ can be corrected in a similar fashion when it is determined from the intensity at zero angle. The procedure holds good for the Guinier region, since again the convolution introduces only a constant multiplier $C_M$ [16].

The scattering curves for spectrin dimers and tetramers are shown in figs. 3 and 4, respectively. The Guinier region lies within the angular range occluded by the beam stop and is therefore inaccessible. When the results are analyzed by way of a cross-section plot, the data can best be fitted by a straight line (figs. 5 and 6 for dimers and tetramers, respectively), from which $R_c$ for spectrin dimers was found to be $14 \pm 1$ Å (averaged over all measurements for both sides of the scattering curve). A value of $12.3 \pm 1$ Å was similarly obtained for the tetramers.

To test our experimental analysis $R_c$ was determined for self-associated glutamate dehydrogenase [18] and found to be 30.6 Å in agreement with Sund et al. [19]. The glutamate dehydrogenase measurements were used to determine $KI_o$ for our instrument based on the published value of

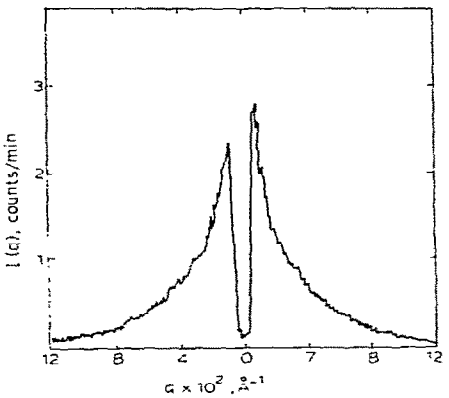


Fig. 3. X-ray scattering curve for spectrin dimers. The sample-to-detector distance was 78 cm; protein concentration 4.6 mg/ml.

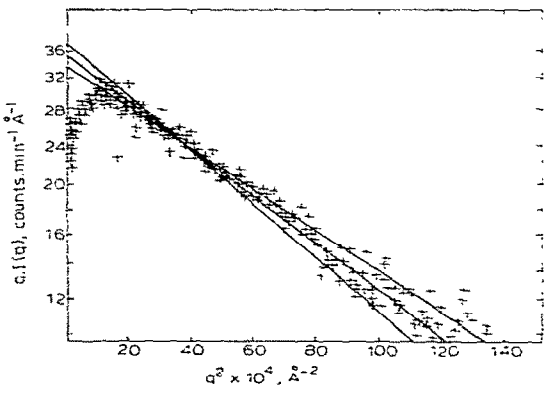


Fig. 5. Cross-section plot of raw data for spectrin dimers. Also shown are the line of best fit to the data, which gives $R_c$ and the lines corresponding to a deviation of ± 1 Å from this value.

the molar mass per unit length ($M/L = 2340$ g mol$^{-1}$ Å$^{-1}$) obtained by absolute calibration [19], using the known apparent specific volume of glutamate dehydrogenate ($\phi' = 0.753$ ml/g) and the measured value of $C_R$ (0.55 for the glutamate dehydrogenase measurements). $KI_0$ was found to be $1.7 \times 10^{-51}$ mol$^{-1}$ l$^{-1}$ g$^{-2}$ el$^{-2}$. $KI_0$ was also determined from measurements of the scattered intensity extrapolated to zero angle of a bovine serum albumin solution, taking the partial specific volume, $\bar{v} = 0.734$ ml/g, with a calculated value of $C_M$ (0.75 for a prolate ellipsoid of eccentricity 2 and $R_g = 30$ Å [20] and our slit geometry). By this procedure, $KI_0$ was found to be $1.5 \times 10^{-51}$ mol$^{-1}$ l$^{-1}$ g$^{-2}$ el$^{-2}$. Using the average of these values of $K$, the molar mass per unit length of spectrin dimers emerged as (590 ± 60) g mol$^{-1}$ Å$^{-1}$ and of spectrin tetramers 530 ± 50 g mol$^{-1}$ Å$^{-1}$ ($\phi' = 0.73$ ml/g).

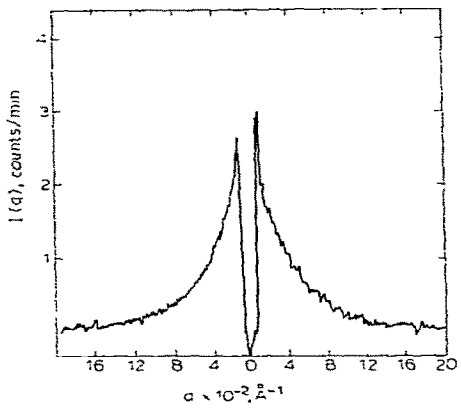


Fig. 4. X-ray scattering curve for spectrin tetramers. Sample-to-detector distance was 50 cm; protein concentration 3.8 mg/ml.

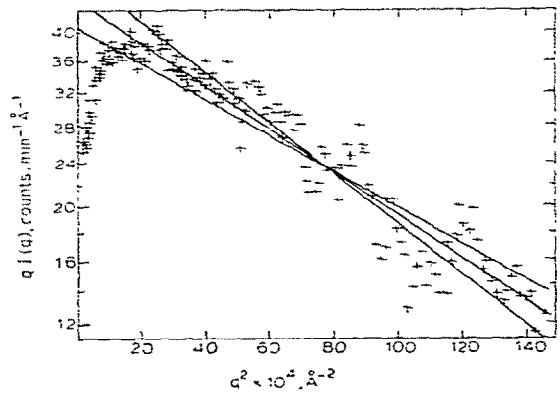


Fig. 6. Cross-section plot of raw data for spectrin tetramers. Also shown are the line of best fit to the data, giving $R_c$, and those corresponding to deviations of ± 1 Å.

### 3.3. Neutron scattering

The neutron scattering curves for the two concentrations of spectrin dimers (4.2 and 1.6 mg/ml) were the same within statistical error after subtraction of the background scattering of the $^2H_2O$ buffer. The curve for spectrin dimers (4.2 mg/ml) is shown in fig. 7. A radius of gyration for the dimers of 174 ± 13 Å was obtained from a Guinier plot of the data from the smallest angles while a cross-section plot for larger angles gave a slope corresponding to $R_c = 45$ Å.

The distance distribution function [16] of the dimers was calculated by Fourier inversion of the scattering data:

$$P(R) = (R/2\pi)^2 \int_0^\infty qI(q) \sin(qR) dq \quad (8)$$

For this calculation, the X-ray and light scattering data were matched to the neutron scattering (see fig. 8) so that the range of scattering vectors included in the analysis could be extended. Light scattering data were fitted by a Gaussian of the form $I(q)/I(0) = \exp(-170^2q^2/3)$ with $q \leq 0.0068$. The neutron scattering data, normalized to $I(q)/I(0)$, extended to $q = 0.027$. Beyond this point the X-ray data were appended to the combined scattering curve. To make them compatible, the X-ray data were first deconvoluted using the method of Vonk [21]. The desmearing influences

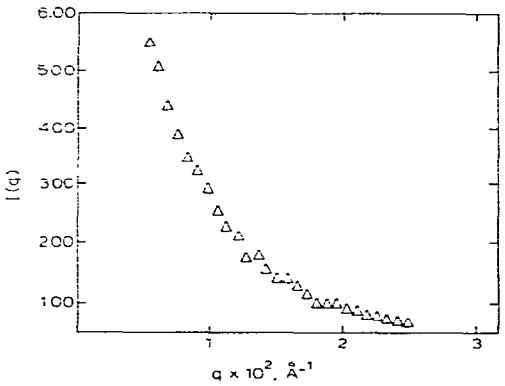


Fig. 7. Plot of raw neutron scattering data for spectrin dimers (protein concentration 4.6 mg/ml).

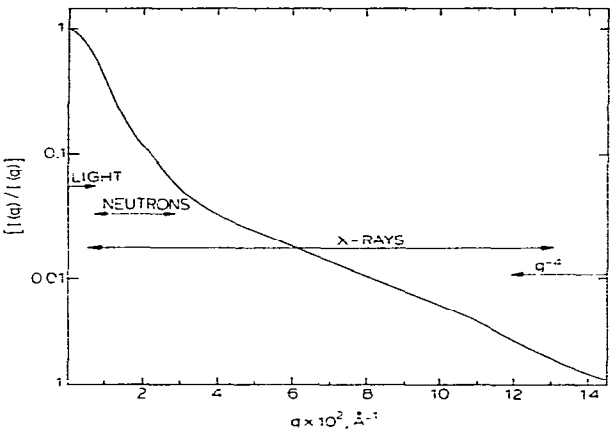


Fig. 8. Consolidated plot of light, X-ray and neutron scattering data for spectrin dimers. The light and X-ray data have been normalized to the neutron data (see text) at the indicated points. The data have been smoothed and the X-ray scattering deconvoluted as indicated in the text.

the data primarily for scattering vectors less than $q = 0.04$. At higher values of $q$, the deconvolution affects the data only by a constant scaling factor. The X-ray data extend to $q = 0.12$, beyond which the $1/q^4$ variation of intensity (Porod extrapolation) was applied. The integration limit was $q = 0.76$ and there was no significant change when it was extended to $q = 1.5$. The distance distribution thus calculated led to a maximum dimension of about 550 Å.

Combination of the X-ray with the light and neutron scattering data in a single curve (fig. 8) lead to a 'calibration' of the absolute intensity of scattered X-rays that is appreciably different from that previously employed. (It may be remarked that this normalization procedure is valid only if the particle contains no large regions that difter markedly in scattering density, for in such a case the shapes of the three scattering curves are apt to be differentially affected by different degrees of contrast in the scattering density.) If the X-ray data, as normalized in fig. 8, are now recast in the form of a cross-section plot, we can obtain the mass per unit length from the relation:

$$M(qI(q)/I(0))_{q\to 0} = \pi(M/L)$$

The value thus obtained (350 g $mol^{-1}$ $Å^{-1}$) is substantially lower than 590 g $mol^{-1}$ $Å^{-1}$ reported above. This may have arisen from errors due to changes in the beam intensity and detector efficiency between different X-ray scattering experiments. In our present system [22] we monitor beam intensity by means of a semi-transparent beam stop which leads to a considerable improvement in the absolute calibration of the X-ray scattering data. Some improvement in the precision of $M/L$ for spectrin can therefore be anticipated in the future.

## 4. Discussion

The structural information derived about spectrin dimers and tetramers by light, neutron and X-ray scattering is summarized in table 1. From the data obtained with the smallest scattering vectors, viz., light and neutrons, the radius of gyration of spectrin dimers was found to lie between 170 and 174 Å. This is very much larger than the value for a spherical molecule of similar molar mass and partial specific volume, which would be about 40 Å. We have therefore applied cross-section analysis to the data, this being appropriate to the treatment of rigid elongated shapes. The cross-section radius of gyration for the dimers was found by X-ray scattering to be about 14 Å. A similar value (12.3 Å) was found for tetramers. For tetramers we determined a radius of gyration of 375 Å (from light scattering), which is close to twice as large as that for the dimer. This must reflect end-to-end association of dimers, in agreement with electron microscopy [1].

Combining the values for mass per unit length of 590 and 350 g $mol^{-1}$ $Å^{-1}$, derived from alternative calibrations of the X-ray scattering data, with the molar mass of 500000 g $mol^{-1}$ $Å^{-1}$, gave contour lengths $L_c$ of 850–1430 Å for the dimers. These values are greater than 590 Å, the length of the rigid rod corresponding to a radius of gyration of 170 Å. We also note that this is larger than the maximum dimension (550 Å) of spectrin dimers derived from the distance function. We therefore conclude that spectrin in solution is a bent rod, as also appears from electron microscopy. The cross-section analysis should be applicable to scattering vectors that probe sizes larger than the thickness but smaller than the length of straight scattering particles. A much larger cross-sectional radius of gyration for the dimer (45 Å) was found from the neutron scattering data than from the X-ray data (14 Å). This difference may be supposed to arise from the different ranges of scattering vectors employed. The neutron scattering measurements were made at small scattering vectors which afford a low-resolution view of the molecule, whereas the X-ray measurements at larger scattering vectors give a higher-resolution view. Consequently, for a bent molecule, the cross-sectional scattering from neutrons may reflect mainly the envelope traced by the bending molecule and, at the higher resolution of the X-ray data it can be considered to result from the cross-section of the molecule itself.

Table 1
Molar masses and dimensions of spectrin dimers and tetramers

| | Dimer | Tetramer |
|---|---|---|
| Molar mass | | |
| $M$ ($\times 10^{-6}$) (g/mol) | 0.47 [a] | 1.06 [a] |
| | 0.54 [b] | |
| | 0.50 [c] | |
| Radius of gyration | | |
| $R_g$ (Å) | 170 ± 30 [a] | 375 ± 40 [d] |
| | 174 ± 13 [d] | |
| Cross-sectional radius of gyration | | |
| $R_c$ (Å) | 14 ± 1 [e] | 12.3 ± 1 [e] |
| Mass per unit length, | | |
| $M/L$ (g $mol^{-1}$ $Å^{-1}$) | 590 ± 60 [e] | 530 ± 60 [e] |
| | 350 [f] | |
| Contour length | | |
| $L_c$ (Å) | 850 [g] | 2000 [g] |
| | 1430 [f] | |
| $D_{max}$ (Å) | 550 [h] | – |
| $L$ (Å) | 590 [a] | 1300 [a] |

[a] Light scattering.
[b] Svedberg equation.
[c] Average.
[d] Neutron scattering.
[e] From small-angle X-ray scattering direct calibration (see text).
[f] From combined scattering curve (see text).
[g] From $M/L$ obtained from direct calibration and $M$.
[h] From the distance distribution function (see text).

In the Appendix we demonstrate this feature using model simulations.

In the light of our scattering data we can now examine the consistency of the results of hydrodynamic measurements to be found in the literature. Consider first the dimer. Assuming cylindrical symmetry we calculate a length $L = 590$ Å for the equivalent cylinder from the light scattering radius of gyration of 170 Å. From the recently established values of Tirado and de la Torre [23] for the translational frictional coefficients of closed cylinders and the value of $1.55 \times 10^{-7}$ cm$^2$ s$^{-1}$ for the translational diffusion coefficient [4], we obtain an axial ratio $p = 5.6$ and therefore a hydrodynamic equivalent radius of $r = 53$ Å. This is in excess of the value of 20 Å for the radius obtained by X-ray scattering from $R_c$, assuming a circular cross-section. It is in reasonable accord with the result obtained by neutron scattering and is believed to correspond to the envelope traced by a bending molecule. The reduction in length from between 850 and 1430 Å to 590 Å thus manifests itself in a corresponding increase in the hydrodynamic equivalent radius. A similar calculation can be performed for the sedimentation coefficient but no additional information about the frictional coefficients can be derived. Consistency is established in that the Svedberg equation yields the correct molar mass [4].

We may now use the dimensions obtained to estimate an intrinsic viscosity $[\eta]$ for the dimer. We use the formulation of Kuhn et al. [24], viz.,

$$[\eta] = (N_A/6)(f_{rot}/M)F(p)$$

where $\eta$ is the viscosity of the medium, $f_{rot}$ the rotational frictional coefficient and $F(p)$, the form factor for elongated ellipsoids of rotation, decreases from 2.5 at $p = 1$ to 0.8 at large values of $p$ (loc. cit. fig. 40, eq. (A 4.15)). The value of $f_{rot}$ is calculated from the recent work of Tirado and de la Torre [25] for rotational friction of a cylindrical particle with the given dimensions. We obtain $[\eta] = 42$ ml/g, which is to be compared with the experimental values of 36 ml/g [26] and $40 \pm 6$ ml/g [27] obtained under comparable experimental conditions.

For the tetramer we calculate a length of 1300 Å for the equivalent cylinder from the light scattering radius of gyration $R_g = 375$ Å. With $D = 1.16 \times 10^{-7}$ cm$^2$ s$^{-1}$ [4], we calculate (as described above) $p = 24$, and the radius, $r = 27$ Å. The axial ratio is considerably in excess of twice that (5.6) of the dimer and this poor agreement reflects the limitations of the model used in the hydrodynamic analysis. We calculate $[\eta]$, which in distinction to translational diffusion is less sensitive to molecular radius, to be 75 ml/g. This is in good agreement with the experimental value of 79 ml/g [27].

It is clear, both from the 2-fold increase in radius of gyration and from the increase in $[\eta]$, that dimers associate head-to-head in forming the tetramer. We prefer to describe the spectrin conformation as kinked or bent, rather than flexible (as suggested by some authors), since a 'flexible' molecule would display a relative contraction upon doubling of the molecular contour length. Such is the case for a persistent, worm-like chain, which undergoes a transition from a rod-like to a Gaussian coil-like state with increasing molecular contour length (cf. fig. 1 of ref. 28). At all events, by the use of the methods so far employed, flexibility cannot be rigorously excluded, but its presence is no more than conjectural.

We consider, finally, the effect of ionic strength on spectrin conformation. The frictional coefficient of spectrin increases markedly at low salt concentrations. For example, according to Stokke and Elgsaeter [27], the intrinsic viscosity of the dimer rises to $78 \pm 8$ ml/g and that of the tetramer to $180 \pm 10$ ml/g at very low ionic strength. If we take it that, as postulated by these authors, electrostatic repulsion under these conditions leads to considerable straightening of the molecule, we may then calculate $L$ from $[\eta]$ on the basis of the considerations outlined above and taking $r = 20$ Å for the stretched cylinder. For the dimer we obtain $L = 1060$ Å and for the tetramer $L = 1960$ Å, which approximate well the respective contour lengths, $L_c$. Elgsaeter [5] also reported light scattering radii of gyration for the heterodimer. Below 2 mM ionic strength he finds $R_g = 450$ Å from which we obtain $L = 1560$ Å for a cylindrical model. This is above the range of estimated contour lengths for the heterodimer (850–1430 Å) and these measurements should therefore be repeated

with a small-angle light scattering technique, more particularly because Elgsaeter's data allow $R_g$ to increase without limit as the ionic strength decreases.

In summary, we conclude that the visual impression of the spectrin dimer and tetramer derived from electron micrographs is in substantial accord with the results of a variety of solution scattering and hydrodynamic data. It also vindicates the conclusions of Clarke [29] from the earliest observations on spectrin in solution.

## Appendix

Here we analyze the scattering from a bent elongated particle. For simplicity we take as a model an assemblage of contiguous spheres of diameter 40 Å arranged in two helical turns of radius $R_h$ (fig. 9). The scattering profile was calculated using the Debye formula for the scattering from an assembly of spheres:

$$I(q) = \phi^2(qR) \sum_n \sum_m \sin(qr_{mn})/qr_{mn}$$

where $\phi(x) = 3(\sin x - x \cos x)/x^3$ is the scattering function for a single sphere, $R$ the radius of each sphere and $r_{mn}$ the centre-to-centre distance for spheres $m$ and $n$.

In fig. 9 the results for a set of values of $R_h$ are shown on a cross-section plot. For small values of $R_h$ a single linear region appears, as expected for a rod in the range of scattering vectors $1/R_g < q < 1/R_c$. For larger values of $R_h$ a steep linear region appears at small angles. At larger angles, interference between helical turns results in oscillations that are superimposed upon the same slope found for $R_{h=0}$. Both the slope of the steep linear region and the size of the oscillations increase as $R_h$ increases.

The linear regions were best fitted using linear regression to obtain the radii of gyration of the cross-section and zero angle intercepts of $\log(qI)$. It was found that $R_c$ (12.7 Å) obtained from the slope of the cross-section plots for small values of $R_h$ (0–40 Å) was identical to that expected for a sphere of diameter 40 Å. For larger $R_h$ the steep inner region gave $R_c$ approximately commensurate with $R_h$ while the outer region was fitted over an angular region, larger than the angular size of the oscillations, to give an $R_c$ value close to that obtained for small $R_h$.

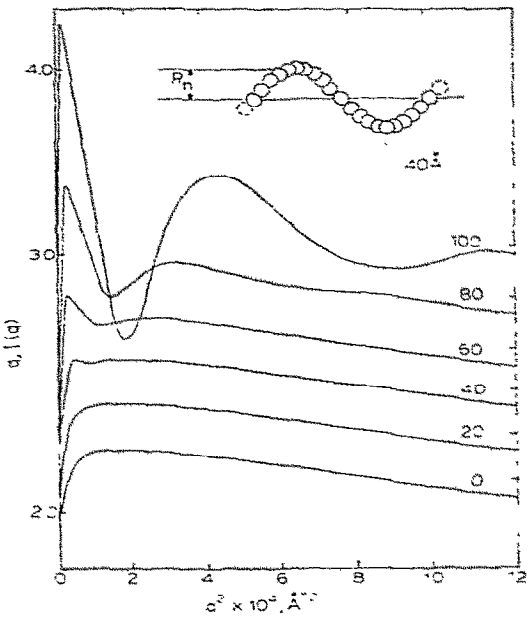


Fig. 9. Cross-section plots of calculated scattering from the helical models described in the Appendix. The numbers at the right and above each curve are the radii $R_h$ of the helices in Å. For clarity successive curves are displaced vertically by an amount indicated on the right-hand ordinate. The geometry of the helical model is shown as an inset.

These results can be interpreted in terms of the maximum resolution in the range of scattering vectors over which the data are fitted. For a helical molecule the scattering at small scattering vectors 'views' the molecule at low resolution and the radius of gyration of the cross-section reflects the helix diameter. The corresponding mass per unit length, obtained from the zero angle extrapolation of the steep slope, indeed equals the total mass divided by the end-to-end extension of the molecule. Thus, for $R_h = 100$ Å we find $R_c = 102$ Å and a mass per unit length 1.5-times that expected for a rod of the same contour length. The calculated end-to-end extension of the above helix was calculated geometrically to be 1/1.6-times the con-

tour length. At larger scattering vectors the slope gives the local cross-section and the zero angle intensity extrapolated from this slope was found to equal the total mass divided by the contour length.

These calculations thus support the qualitative interpretion of the $R_c$ values obtained from neutron as compared with X-ray scattering from spectrin described in the text.

## Acknowledgement

We thank Reuven de Roos for his many contributions to the development of the X-ray scattering system.

## References

1 D.M. Shotton, B. Burke and D. Branton, J. Mol. Biol. 131 (1979) 303.
2 D. Branton, C.M. Cohen and J. Tyler, Cell 24 (1981) 24.
3 J.M. Tyler, J.M. Anderson and D. Branton, J. Cell Biol. 85 (1980) 489.
4 Z. Kam, R. Josephs, H. Eisenberg and W.B. Gratzer, Biochemistry 16 (1977) 5568.
5 A. Elgsaeter, Biochim. Biophys. Acta 536 (1978) 235.
6 E. Ungewickell and W.B. Gratzer, Eur. J. Biochem. 88 (1978) 379.
7 R. Calvert, E. Ungewickell and W.B. Gratzer, Eur. J. Biochem. 107 (1980) 363.
8 D. Jolly and H. Eisenberg, Biopolymers 15 (1976) 61.
9 A. Franks, Proc. Phys. Soc. B 68 (1955) 1054.
10 H. Eisenberg, in: Procedures in nucleic acid research, vol. 2, eds. G.I. Cantoni and D.R. Davies (Harper and Row, New York, 1971) p. 137.
11 A. Guinier, Ann. Phys. 12 (1939) 161.
12 H. Eisenberg, Q. Rev. Biophys. 14 (1981) 141.
13 H. Pessen, J.F. Kumosinski and S.N. Timasheff, Methods Enzymol. 27 (1973) 151.
14 H. Eisenberg, Biological macromolecules and polyelectrolytes in solution (Oxford University Press, London, 1976).
15 W.W. Beeman, P. Kaesberg, J.W. Anderegg and M.B. Webb, Handb. Phys. 32 (1957) 321.
16 A. Guinier and G. Fournet Small angle scattering of X-rays (J. Wiley and Sons, New York, 1955).
17 G. Fournet, Bull. Soc. Fr. Mineral. Crist. 74 (1951) 39.
18 H. Eisenberg and E. Reisler, Biopolymers 10 (1971) 2363.
19 H. Sund, I. Pilz and M. Herbst, Eur. J. Biochem. 7 (1969) 517.
20 J.W. Anderegg, W.W. Beeman, S. Shulman and P. Kaesberg, J. Am. Chem. Soc. 77 (1955) 2927.
21 C.G. Vonk, J. Appl. Crystallogr. 4 (1971) 340.
22 M.H. Reich, Z. Kam and H. Eisenberg, Biochemistry 21 (1982) in the press
23 M.M. Tirado and J.G. de la Torre, J. Chem. Phys. 71 (1979) 2581.
24 W. Kuhn, H. Kuhn and P. Buchner, Ergeb. Exakten. Naturwiss. 25 (1951) 1.
25 M.M. Tirado and J.G. de la Torre, J. Chem. Phys. 73 (1980) 1986.
26 J.C. Dunbar and G.B. Ralston, Biochim. Biophys. Acta 667 (1981) 177.
27 B.T. Stokke and A. Elgsaeter, Biochim. Biophys. Acta 640 (1981) 640.
28 Z. Kam, N. Borochov and H. Eisenberg, Biopolymers 20 (1981) 2671.
29 M. Clarke, Biochem. Biophys. Res. Commun. 45 (1971) 1063.